Title: Pushed to the edge: hundreds of Myosin 10s pack into filopodia and could cause traffic jams on actin

Julia Shangguan[1], Ronald S. Rock[1,2*]

[1]Department of Biochemistry and Molecular Biology, [2]Institute for Biophysical Dynamics, The University of Chicago, Chicago, Illinois, USA
*To whom correspondence should be addressed: rrock@uchicago.edu

Abstract

Myosin 10 (Myo10) is a vertebrate-specific motor protein well known for its role in filopodia formation. Although Myo10-driven filopodial dynamics have been characterized, there is no information about the numbers of Myo10 in filopodia. To better understand molecular stoichiometries and packing restraints in filopodia, we measured Myo10 abundance in these structures. Here we combined SDS-PAGE analysis with epifluorescence microscopy to quantitate HaloTag-labeled Myo10 in U2OS cells. About 6% of total intracellular Myo10 localizes to filopodia, where it tends to be enriched at opposite ends of the cell. Hundreds of Myo10 are found in a typical filopodium, and their distribution across filopodia is log-normal. Some filopodial tips even contain more Myo10 than accessible binding sites on the actin filament bundle. Our estimates of Myo10 molecules in filopodia provide insight into the physics of packing Myo10, its cargo, and other filopodia-associated proteins in narrow membrane deformations in addition to the numbers of Myo10 required for filopodia initiation. Our protocol provides a framework for future work analyzing Myo10 abundance and distribution upon perturbation.

Introduction

Myosins are a group of motor proteins that travel along the cell's dynamic cytoskeletal highways, binding actin under ATP regulation. Apart from myosin 2, the other >30 classes are considered 'unconventional' and contain membrane and cargo-binding tails. A myosin of particular interest is myosin 10 (Myo10), a vertebrate-specific motor protein well known for its role in cellular protrusions. These protrusions, termed filopodia, comprise tightly packed, parallel actin filaments and participate in a multitude of processes such as endocytosis, cell migration, and wound healing[1].

Myo10's role in filopodia has been widely investigated[2–14]. Myo10 expression increases dorsal filopodia, and Myo10 overexpression induces many Myo10 tip-localized filopodia[4,15,16]. Estimations on Myo10-positive filopodia length, average number of filopodia per area, and the velocities of extension and retraction have been reported[4,7,15] However, questions regarding the quantity and distribution of Myo10 molecules within the cell still linger. Published images of Myo10 show its prominent localization in the filopodial tip, but a pool of Myo10 in the cell body remains[17,18]. A quantitative understanding of Myo10 localization could provide further insight into Myo10 regulatory factors, and how the crowded environment inside a thin filopodium affects the composition of the filopodial tip complex.

Studies estimating protein numbers in cells have been conducted before[19,20–22]. Methods include super-resolution microscopy[22], mass spectrometry[23], western blots[19], and photobleaching experiments[24]. We describe here a simple imaging and analysis method exploiting HaloTag labeling technology to probe Myo10's contributions to filopodia nucleation and examine its distribution across filopodia. Similar to quantitative Western blotting of GFP[19], our strategy relies on quantitative SDS-PAGE using a fluorescent protein standard to estimate the average number of Myo10 molecules per cell. We then use this value to convert the same fluorescent signal in micrographs to obtain Myo10 quantity in subcellular structures.

We found that the bulk of Myo10 remains in the cell body, with hundreds of Myo10s in each filopodium. Myo10 is unevenly distributed across a cell's filopodia, and some filopodial tips have an excess of Myo10 over accessible actin filament binding-sites. Having relative numbers of Myo10 molecules contextualizes potential stoichiometric ratios of Myo10 and its cargo. This study sets up future work to identify Myo10 activation factors and to analyze the effects of different perturbations on Myo10 density and localization.

Results & Discussion

We measured the quantity of Myo10 molecules within filopodia and visualized its overall arrangement within the cell (Fig. 1A). We produced a human full-length Myo10 construct with a N-terminal HaloTag and C-terminal Flag-tag. Both N-terminal and C-terminal labeled Myo10 have almost identical staining patterns (Supplementary Fig. 1A), so the N-terminal HaloTag was selected for subsequent work. To estimate the number of Myo10 molecules within specific cellular compartments, we combined SDS-PAGE and epifluorescence microscopy. First, we

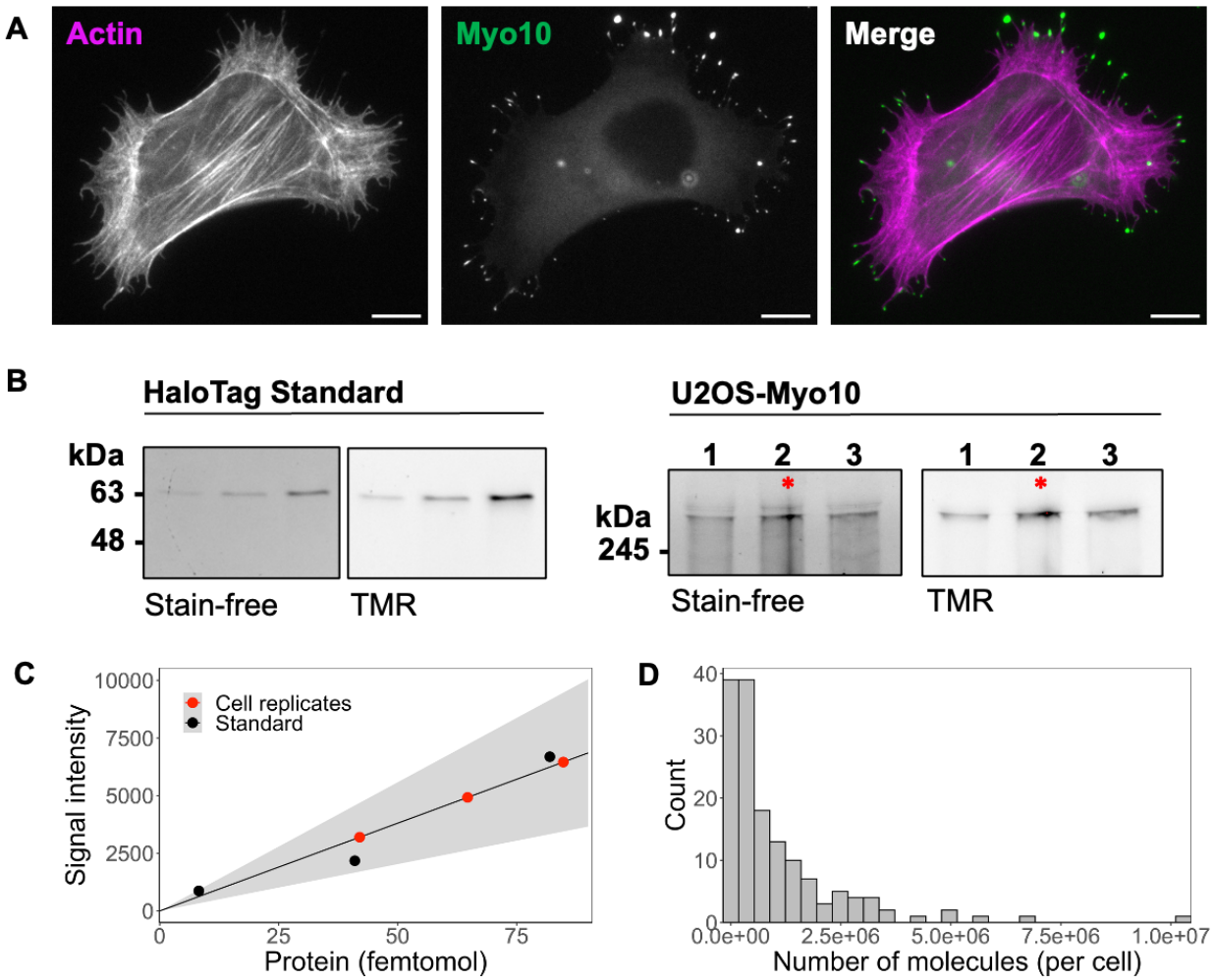

Fig. 1. Hundreds of thousands of Myo10 monomer molecules found in U2OS cells overexpressed with Myo10. (A) Epifluorescence image of exogenously expressed HaloTag-Myo10 in U2OS cells. Actin is labeled with phalloidin-AF633 (magenta). Myo10 is labeled with HaloTag ligand-TMR (green). Scale bar = 10 µm. (B) Left SDS-PAGE lanes: 1, 5, and 10 ng of Halo standard protein were loaded (left to right). Right SDS-PAGE lanes: 40,000 cells from three separate U2OS transient transfections (bioreplicate 1, 2 and 3) were loaded. Stain-free shows total protein signal, and TMR illumination shows only HaloTag-Myo10 signal. Red asterisk (*) indicates aggregate avoided in signal integration. (C) Standard curve for TMR fluorescence signal of Halo Standard Protein (black dots) compared to signal from HaloTag-Myo10 U2OS cells (red dots). y = 76.12x, where the y-intercept is set to 0. R^2 = 0.99. Standard error of slope = 8.25. Grey shading indicates 95% confidence interval. (D) Distribution of the number of Myo10 molecules per cell as determined by quantification of 150 cell images. Min = 30,000 (95% CI: 21,000-57,000), median = 480,000 (95% CI: 330,000-900,00), max =10,000,000 (95% CI: 7,000,000-19,000,000).

loaded lysate from a known number of Myo10-transfected U2OS cells on an SDS-PAGE gel along with known amounts of HaloTag Standard Protein, a 61 kDa HaloTag-GST fusion protein (Fig. 1B-C, Supplementary Fig. 1C). Because all samples were incubated with TMR-HaloTag ligand, we use the standard protein's fluorescence emission in the gel to generate a standard curve and estimate the average Myo10 molecules per cell. We propagate the 95% CI from the

gel standard curve for our subsequent error estimates. In parallel, we measured Myo10 molecules in the U2OS cells using epifluorescence microscopy, obtaining total, background-subtracted fluorescence signal intensity for each of the three, 50-cell biological replicates. We used these totals to determine the fluorescence signal per molecule by microscopy. Both fixed cells and gel samples were labeled with excess HaloTag ligand to ensure maximal labeling of Myo10 molecules with no detectable nonspecific labeling (Supplementary Fig. 1D-E). Measurements from the three bioreplicates were pooled, resulting in the analysis of 150 cells of varying Myo10 expression levels (Fig. 1D). The number of Myo10-positive protrusions per cell ranges from 12 to 116, with a median of 55 (Fig. 2A). Varying filopodia density likely reflects cells at different stages of migration or signaling[7,25].

Despite cells containing a median of 480,000 (95% CI: 330,000-900,000) total Myo10 molecules (Fig. 1D), only a small proportion of Myo10 localizes to filopodia (median 5.4%, Fig. 2B). Available PtdIns(3,4,5)P_3 in the cell could be limiting the portion of free intracellular Myo10 that is activated and entering filopodia. Umeki et al. proposed that Myo10 binds PtdIns(3,4,5)P_3 at cell peripheries and dimerizes, becomes activated and converges local actin filaments to form the filopodial base[26]. Thus, the number of Myo10 molecules in filopodia could be limited by the rate of Myo10 activation. Although Myo10 can participate in filopodia formation independently of VASP proteins and substrate attachment [4], other proteins have been found to be conserved in mechanisms of filopodia initiation. Components such as Cdc42[27], formin[28], Arp2/3 complex[29], neurofascin[25] or VASP[30] could be prospective limiting partners of Myo10 entry into filopodia.

Mechanisms of Myo10 activation could be revealed by its spatial correlation. Interactions with membrane-bound proteins or small cytosolic factors impact where Myo10 is localized. Indeed, Myo10 is not equally distributed, instead concentrating in select cellular zones and at opposite ends of the cell (Fig. 2C & D, Supplementary Fig. 2). Cells display periodic stretches of higher Myo10 density along the cell membrane, and some cells even contain membrane regions devoid of filopodia and Myo10 (Supplementary Fig. 2). Fast targeting of Myo10 to certain filopodial tips can be summarized by a 3D -> 2D -> 1D reduction in dimensionality[31]. The bulk of Myo10 in the cell body undergoes rapid diffusion in 3D space. Weak binding between Myo10's motor domain and PH domains to bundled actin filaments and PtdIns(3,4,5)P_3, respectively, immobilizes Myo10 at the plasma membrane. Slowed 2D diffusion along the

plasma membrane eventually leads to filopodia initiation. At the filopodium base, Myo10 shows directed entry into the shaft, where it processively walks along the actin bundle to the tip.

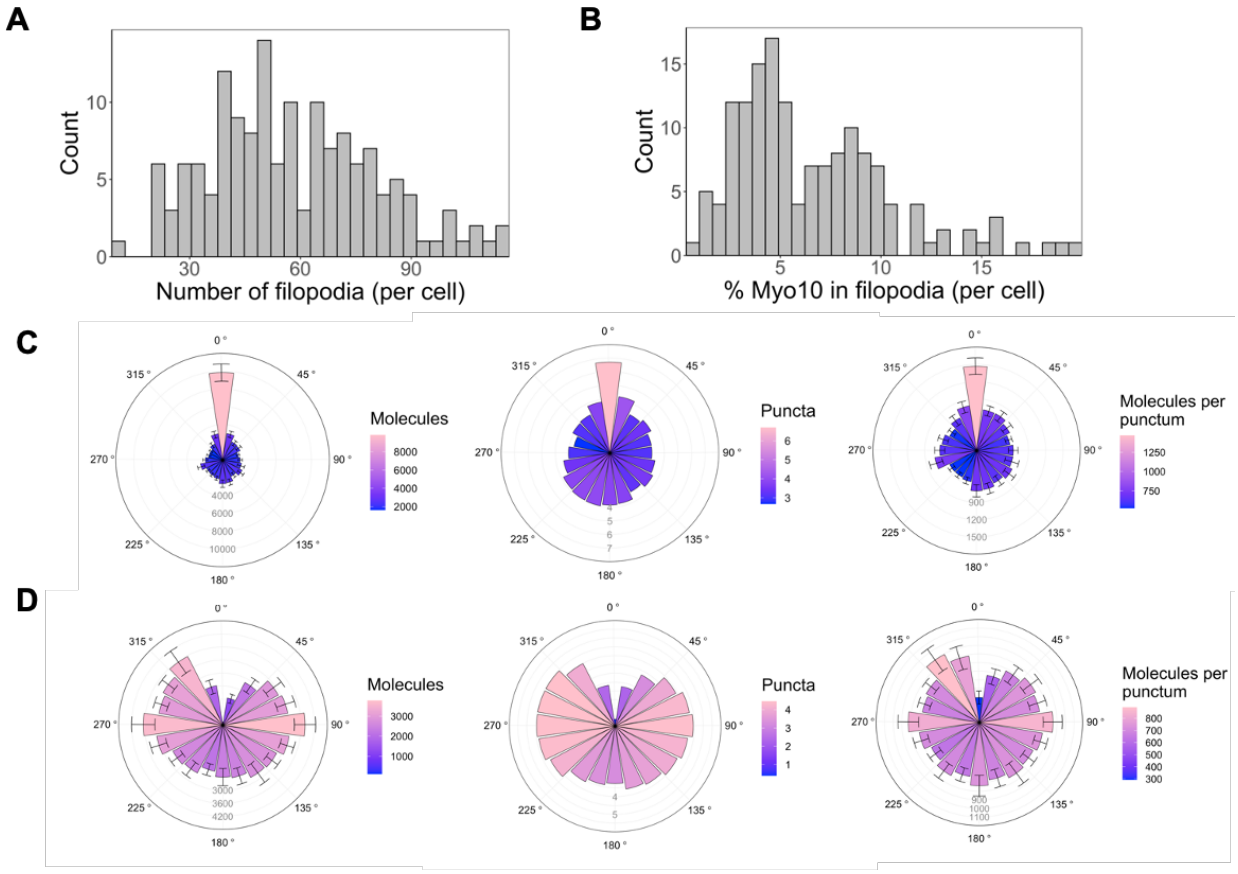

Fig. 2. Only a small portion of intracellular Myo10 is activated and enters filopodia, and Myo10 is not evenly distributed along the cell edge. (A) Distribution of the number of Myo10-positive filopodia per cell. Min = 12, median = 55, max = 116. Total of 8,733 Myo10-positive filopodia were analyzed. (B) Distribution of the percent of Myo10 localized in the filopodia per cell as determined by quantification of 150 cell images. Min = 0.9%, median = 5.4%, max = 19.9%. (C) Spatial correlation of Myo10-rich regions of the cell edge. Each cell was divided into 20 angular sections, and the section with the most molecules was aligned to 0°. Section quantities were then averaged across cells. Molecules, puncta, and molecules per punctum are shown. (D) Spatial correlation of Myo10-poor regions of the cell edge. As in (C), but the section with the fewest molecules was aligned to 0° for each cell's rose plot. If >1 section contained no Myo10, a randomly selected empty Myo10 section was aligned to 0°. Error bars in C, D are the standard error of the mean for 500 bootstrapped samples of the 150 cells. Note the correlation of both molecules and puncta at opposite ends of cells (0°, 180°), and the anticorrelation with the two sides (90°, 270°).

Filopodia containing high Myo10 signal are surrounded by more neighboring filopodia, as evidenced by increased numbers of proximal Myo10 puncta (Fig. 2C, center). The number of Myo10 per filopodium appears random and relatively fixed because the number of molecules per punctum is consistent (Fig. 2C, right). Potentially a local activation signal initiates filopodia at a particular site, and then the signal spreads from the high Myo10 zone to generate more puncta in the immediate vicinity. The opposite is weakly true, by which filopodia with low Myo10 levels

tend to be next to fewer Myo10 puncta (Fig. 2D, center). We hypothesize a few different explanations for why Myo10 is not equally distributed along the membrane. Potentially Myo10 is funneled into filopodia that are moving towards specific environmental stimuli that simultaneously affect Myo10[32,33]. Alternatively, Myo10 could be responding to information encoded in the actin itself or other molecules present in certain filopodia. Myosins can differentiate the structural and chemical properties of actin filament types (e.g. age, tension, curvature, post-translational modifications) based on changes in its kinetics and thermodynamics upon interaction with actin, and depending on where the actin is located[34]. Thus, actin filament networks could be partly responsible for choreographing Myo10 trajectories[34]. Future studies could identify potential guidance cues that Myo10-positive filopodia are responding to and

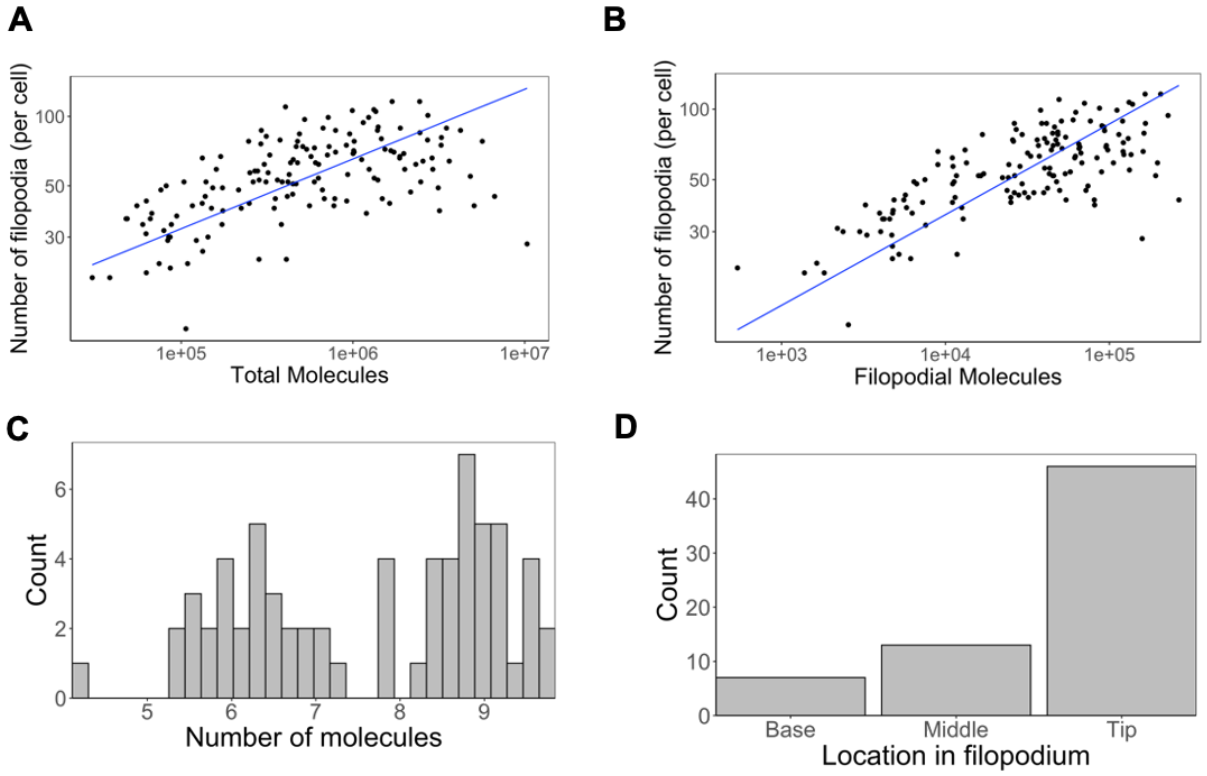

Fig. 3. Tens of Myo10 are sufficient to nucleate filopodia. (A) Correlation between number of Myo10-positive filopodia in a cell and the total number of Myo10 molecules in the cell. The slope of power law function is 0.30. (B) Correlation between number of Myo10-positive filopodia in a cell and the number of filopodial Myo10 molecules in the cell. The slope of power law function is 0.39. (C) Dim Myo10 puncta in filopodia, identified as those containing <10 Myo10 molecules, were examined. 135 total dim puncta across 26 cells were identified. Of the 135 puncta, 7 puncta were hard to visually interpret, 7 puncta were image noise, and 56 puncta were over-segmented (e.g. not actual distinct puncta but rather part of continuous Myo10 signal in filopodia). The distribution of the remaining 66 true dim puncta is displayed. (D) Filopodial localization of dim Myo10 puncta containing <10 molecules. The 66 true dim puncta from (C) were analyzed.

identify other signaling proteins enriched in filopodia with high Myo10 signal. It is unclear how myosins navigate to the right place at the right time, but our results support an important interplay between Myo10 and the actin network.

What does a cell's total Myo10 filopodial signal indicate about filopodia formation? Having higher Myo10 filopodial signals tends to correlate with more filopodia, but the trend eventually does plateau (Fig. 3A). Having higher total intracellular Myo10 weakly correlates with more filopodia (Fig. 3B), which supports our earlier hypothesis that other components necessary for filopodia initiation could be rate-limiting. Myo10 alone is likely not sufficient for filopodia formation, instead, it needs an activation source. Once activated, we hypothesize that only ten or fewer Myo10 molecules are necessary for filopodia initiation (Fig. 3C). As noted earlier, Myo10 is not equally distributed along the filopodium shaft: it is often concentrated into distinct puncta (Fig. 1A). We noticed that a filopodium can form from a single punctum of around ten Myo10 molecules, and dim Myo10 puncta are often tip-localized (Fig. 3D). The median number of Myo10 molecules per filopodium is ~ 360 molecules (95% CI: 240-670; 8733 total filopodia) (Fig. 4 A & B).

Our findings can help us begin to understand the Myo10 concentrations found in filopodia, and how that quantity relates to the amount of available actin sites for binding. To estimate Myo10 concentrations in filopodia, we used published values to define the geometry of a "typical" filopodium [35,36,37]. Considering a filopodium to be a cylindrical tube, we calculated local concentrations of Myo10 at filopodial tips using the length of a Myo10 punctum as the height, and a fixed radius of 100 nm[38]. At the tips, Myo10 ranges from ~ 3 μM to 225 μM. Its distribution among filopodia is apparently log-normal (Fig. 4C, Supplementary Fig. 3).

The vast range of Myo10 molecules per filopodium stands in contrast to more consistent, normally-distributed quantities of other actin-binding proteins. In fission yeast, proteins in the spindle pole body (e.g. Sad1p), at the cytokinetic contractile ring (e.g. Myo2p, Rho GEF Rgf1p), and within actin patches (e.g. ARPC1, capping protein Acp2p) did not display the wide concentration ranges that we saw for Myo10 in filopodia[19]. We speculate several reasons for the non-Gaussian distribution of Myo10 molecules. Log-normal distributions are commonly associated with growth processes, and the accumulation of Myo10 at filopodial tips fits this description. Filopodia have a large capacity for additional Myo10, and an ample reserve of unactivated Myo10 remains in the cytosol. Thus, filopodia operate in a non-saturated state,

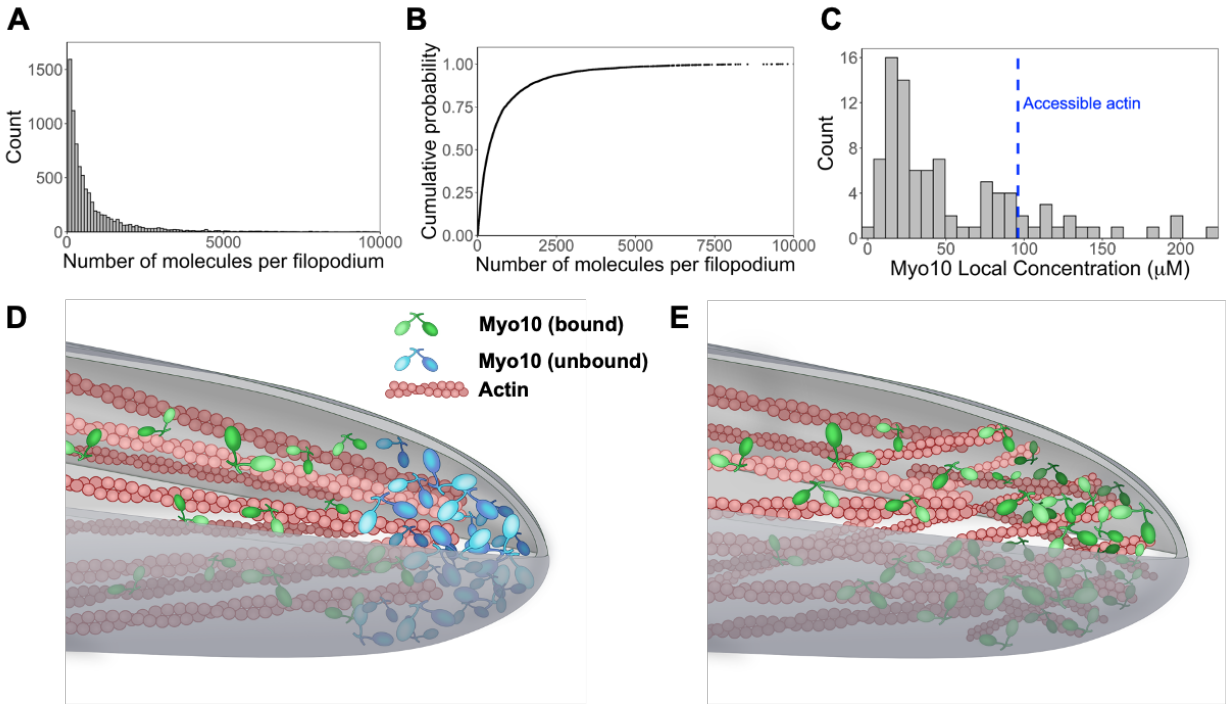

Fig. 4. Hundreds of Myo10 monomer molecules found in a filopodium, potentially in excess over available actin at the filopodium tip. (A) Distribution of the number of Myo10 molecules per filopodium as determined by quantification of 150 cell images. Min = 2 (95% CI: 1-4), median = 360 (95% CI: 240-670), max = 63,000 (95% CI: 43,000-120,000). 59 data points with values >10,000 molecules were excluded from plotting. 8,733 total filopodia. (B) Cumulative distribution function plot of Myo10 molecules per filopodium. 59 data points with values >10,000 molecules were excluded from plotting. 8,733 total filopodia. (C) The length of 90 randomly chosen filopodia tip-localized Myo10 puncta were measured in ImageJ. The volume occupied by the Myo10 punctum was estimated using the volume of a cylinder, where length = height and width = 2*radius. Radius for all Myo10 puncta was treated as 0.1 μm (published average) since resolution limit ~250 nm. The signal intensity of the Myo10 punctum was converted to molecules to obtain local concentration (in μM). Min = 3.2 (95% CI: 2.1-6), median = 35 (95% CI: 24-65), max = 220 (95% CI: 150-420). 9 different cell images were analyzed in total. Blue dashed vertical line indicates the concentration of F-actin accessible for Myo10 binding in a filopodium (~96 uM). (D) Model of a Myo10 traffic jam at the filopodium tip. Not enough available actin monomers results in a population of free and unbound Myo10. (E) Model of frayed actin filaments at the filopodium tip. If actin filaments are not neatly packed into parallel bundles at the filopodium tip, disorganized and frayed actin filaments yield more accessible binding sites to Myo10.

enabling unrestricted Myo10 accumulation. In contrast, we suspect that the spindle pole body, cytokinetic ring, and actin patches represent cytoskeletal systems constructed from one or more limiting reagents. Limiting reagents put an upper bound on the growth of the system and lead to normal distributions at saturation. Furthermore, the end requirements of cytokinesis and filopodial formation differ. Cytokinesis is a tightly regulated process involving a balance of forces, and the precise timing of each stage has been described in fission yeast[39]. Disruptions to components of the contractile ring, such as myosin inhibition, affect rates of actin filament disassembly and ring constriction[20]. In contrast, there is no specific number of filopodia that cells aim to create nor is there an optimal number of Myo10 per filopodium. Therefore, filopodia

formation is a much more permissive process than cytokinesis, which could also explain the variation in values we observe of Myo10 compared to contractile ring-associated proteins.

Interestingly, there is an activation mechanism that continues to push Myo10 into the filopodia, even when there may not be available actin to bind. To estimate the amount of F-actin available for binding, we modeled a filopodium of radius 100 nm comprising 30 actin filaments, of which 16 filaments are on the exposed surface of the bundle. Nagy et al. (2010) posited that only 4 of the 13 actin monomers per helical turn are available to Myo10 binding because of Myo10's stepping behavior[36]. Using Zhuralev et al.'s equation[37] for calculating F-actin monomer concentration in a filopodium, we estimate that ~96 uM of actin monomers are available for Myo10 binding (see Supplementary Fig. 4 for full calculations).

If a filopodium contains ~96 μM of F-actin available to Myo10 (Supplementary Fig. 4), and up to 225 μM Myo10, then sometimes Myo10 appears in excess. This would inevitably lead to a molecular traffic jam within the filopodia. When there is no space available to walk on actin, what mechanism continually activates and drives Myo10 into filopodial tips? Further studies are needed to elucidate the details of Myo10 activation. Alternatively, the ends of actin bundles could be frayed at filopodial tips, increasing the available binding spots for Myo10[40]. The consequences of Myo10 traffic jams and actin fraying on the dynamics of actin itself and the activity of its associated proteins remain unknown.

Although our experiments were conducted with the intention of minimizing biases and errors, our results do come with caveats. We added excess HaloLigand to saturate HaloTag-Myo10 in cells, but the labeling efficiency of Halo-tagged Myo10 could be less than 100%. U2OS cells express low levels of Myo10, so there is a small population of unlabeled endogenous Myo10 unaddressed by this paper. Both of these errors would lead to an underestimation of Myo10 in filopodia, amplifying our estimates of excess Myo10 at the tip (Supplementary Fig. 3). Regarding aspects of microscopy and automated image segmentation/processing, very dim Myo10 spots could have escaped detection. Furthermore, our estimates of molecules are predicated on the calibration curve of the Halo Standard Protein on the SDS-PAGE gels, which is likely the highest source of error on our molecule counts. Despite these concerns, our values still provide a sense of the magnitude of Myo10 molecules within cellular structures.

Knowing the number of Myo10 molecules in a filopodium provides insight into molecular packing geometries in confined intracellular spaces. With the combination of

epifluorescence microscopy and SDS-PAGE, we found that filopodia typically contain hundreds of Myo10 molecules. This paper presents the first quantitative analysis of an unconventional myosin in human cells. Our results contribute to understandings of molecular stoichiometries in filopodia and Myo10 abundance in these structures. Our protocol provides a framework for future studies examining the factors that tune Myo10 density and distribution.

Methods

Full-length human Myo10 sequence was constructed in a pTT5 vector backbone plasmid. U2OS cells were passaged every 2 days and used under passage number 5. Cells were grown in Gibco 1x DMEM (ThermoFisher, 11995073) supplemented with 10% fetal bovine serum prior to transfection. Cells were transiently transfected with 1 ug of the HaloTag-Myo10-FlagTag plasmid and 0.2 µg of a calmodulin plasmid using FuGENE HD Transfection reagent. Forty-eight hours after transfection, cells were detached using Accutase and seeded onto ibidi 8 well chamber slides coated with 20 µg/ml laminin for imaging and onto 6 well dishes for SDS-PAGE analysis. After 3-4 hours, cells were collected for SDS-PAGE analysis at the same time as cells were fixed for microscopy. Three bioreplicates were conducted.

For Myo10 imaging, cells were fixed for 20 min in a solution comprising: 4% PFA, 0.08% Triton, 2.5 µM TMR-HaloLigand, and 1:1000 DAPI in PEM buffer. After 3 PBS washes (4 min each), cells were stained with 1 mM Phalloidin-AF633 in 1% BSA for 20 min. Cells were washed 3x with PBS (4 min each) before immediate imaging. Fluorescence images were taken on an Axiovert using a gain of 125 and 175 ms exposure (below detector saturation). To prevent photobleaching, cells were kept in the dark and imaged immediately upon illumination of the selected field of view. Samples were imaged within a day of preparation. TMR was visualized using green light and AF633 was visualized with red light.

For SDS-PAGE analysis, cells growing in the 6 well plate were first incubated with Accutase containing 3 µM TMR-HaloLigand for 15 min at room temperature in the dark. Accutase was neutralized with DMEM +10 % FBS and the cells were collected with a 3:30 min spin at 400 rcf at room temperature. The pellet was resuspended in 100 µl cell media, and 10 µl of the cells were removed and mixed with 1x Trypan blue for cell counting. The remaining cells were combined with 400 µl cell media and subjected to a 5 min, 400 rcf spin at room temperature. Cells were moved to ice post-spin and lysed in RIPA buffer containing 1 mM

PMSF. Halo Standard Protein (Promega, G4491) samples were prepared for final masses of 1 ng, 5 ng, and 10 ng and lysate samples containing 40,000 cells on the gel. Excess TMR-HaloLigand was incubated with samples for 5 minutes. All samples were boiled at 70°C for 10 min before loading onto a 4-20% Mini-PROTEAN TGX Stain-Free protein gel (BioRad, 4568095). The gel was run at 180 V for 45 min and imaged on a ChemiDoc. Images of the stain-free, AF647, and rhodamine channels were taken. We used the Gel Analysis plugin in ImageJ to compare signal intensity of the gel bands. Signal was only integrated for the left half of the lanes to avoid an aggregate in bioreplicate 2. We justify this analysis for the following reasons: total protein signal in the stain-free channel was equivalent for the half-lane integrations of the 3 bioreplicates, and half-lane integrations of the HaloStandard lanes were directly half signal of its full-lane integrations. A standard curve was generated from the Halo Standard Protein signal to estimate the number of Myo10 molecules per total cells loaded, with a value correction accounting for positively transfected cells. Microscopy was used to count the percentage of transfected cells from ~105-130 randomly surveyed cells per bioreplicate.

Image analysis was done using in-house Python scripts. To calculate the number of Myo10 molecules in the fluorescence images, the Myo10-stained images were first background subtracted: the average signal of a 56 x 56 pixel square near the cell body was calculated and subtracted from each pixel of the TIFF image. Next, the phalloidin-stained cell image and Myo10-stained image were filtered to remove non-cell objects and subjected to watershed segmentation. To generate a 'cell body mask', an erosion function followed by an opening function were applied to the phalloidin-stained cell image. The Myo10 image mask was defined as the 'total cell mask.' The 'cell body mask' was subtracted from the 'total cell mask' for a 'filopodia mask.' Connected component analysis was performed on the 'filopodia mask' to obtain masks for all filopodia-localized Myo10 puncta and then inspected in Napari[41]. Puncta belonging to the same filopodium were manually combined into the same filopodium mask. Signal in each filopodium mask and within the 'cell body mask' were summed. For each bioreplicate, a 'total pool' of Myo10 molecules was calculated by multiplying the average Myo10 molecules per cell by the number of cell images analyzed. Within each bioreplicate, the signal intensities were summed for all cells. Therefore, to get the number of molecules within a Myo10 filopodium, the filopodium intensity was divided by the bioreplicate signal intensity sum

and multiplied by 'total pool.' To calculate percentage of Myo10-positive filopodia, total filopodia per cell were manually counted.

To generate the rose plots of the Myo10 distribution in filopodia, each cell was divided into 20 radial sections from the cell's center of mass. The Myo10 filopodial molecules were averaged within each section. The section with the highest molecules was aligned to degree 0 for each cell's rose plot. Total count of Myo10 puncta analyzed per section was also calculated. Puncta were not manually combined if belonging to the same filopodium. Therefore, puncta that were at the border of two radial sections were counted once for each section. For the rose plots in panel 2D, a randomly selected empty Myo10 section was aligned to degree 0 if more than one section contained no Myo10. The standard error bars represent the standard error of the mean molecules per section after 500 iterations of bootstrapping. In each iteration, 150 cells were randomly selected with replacement.

To obtain estimates of local Myo10 concentrations in filopodia, 10 Myo10 puncta were randomly chosen from 3 different cell images of each bioreplicate set. The length of each punctum was measured in ImageJ. The volume occupied by the Myo10 punctum was estimated using the volume of a cylinder: length = height and width = 2*radius, where radius was assumed to be 100 nm (reported average radius). The signal intensity of the Myo10 punctum was converted to molecules as described above.

Acknowledgments

We thank Prof. David Kovar, Department of Cell Biology, University of Chicago, for critical comments on the manuscript. This work was supported by the University of Chicago MCB Training Grant (T32 GM144292) and the NSF Graduate Research Fellowship (2140001) (to J.S.) and NIH grants R01GM124272 and R01GM149073 (to R.S.R.).

References Cited

1. Mattila, P. K. & Lappalainen, P. Filopodia: molecular architecture and cellular functions. *Nat Rev Mol Cell Biol* **9**, 446–454 (2008).

2. Zhang, H. *et al.* Myosin-X provides a motor-based link between integrins and the cytoskeleton. *Nat Cell Biol* **6**, 523–531 (2004).
3. Tokuo, H. & Ikebe, M. Myosin X transports Mena/VASP to the tip of filopodia. *Biochemical and Biophysical Research Communications* **319**, 214–220 (2004).
4. Bohil, A. B., Robertson, B. W. & Cheney, R. E. Myosin-X is a molecular motor that functions in filopodia formation. *Proceedings of the National Academy of Sciences* **103**, 12411–12416 (2006).
5. Tokuo, H., Mabuchi, K. & Ikebe, M. The motor activity of myosin-X promotes actin fiber convergence at the cell periphery to initiate filopodia formation. *Journal of Cell Biology* **179**, 229–238 (2007).
6. Zhu, X.-J. *et al.* Myosin X regulates netrin receptors and functions in axonal path-finding. *Nat Cell Biol* **9**, 184–192 (2007).
7. Kerber, M. L. & Cheney, R. E. Myosin-X: a MyTH-FERM myosin at the tips of filopodia. *Journal of Cell Science* **124**, 3733–3741 (2011).
8. Raines, A. N., Nagdas, S., Kerber, M. L. & Cheney, R. E. Headless Myo10 Is a Negative Regulator of Full-length Myo10 and Inhibits Axon Outgrowth in Cortical Neurons. *Journal of Biological Chemistry* **287**, 24873–24883 (2012).
9. Arjonen, A. *et al.* Mutant p53–associated myosin-X upregulation promotes breast cancer invasion and metastasis. *J. Clin. Invest.* **124**, 1069–1082 (2014).
10. Courson, D. S. & Cheney, R. E. Myosin-X and disease. *Experimental Cell Research* **334**, 10–15 (2015).

11. He, K., Sakai, T., Tsukasaki, Y., Watanabe, T. M. & Ikebe, M. Myosin X is recruited to nascent focal adhesions at the leading edge and induces multi-cycle filopodial elongation. *Sci Rep* **7**, 13685 (2017).
12. Heimsath, E. G., Yim, Y.-I., Mustapha, M., Hammer, J. A. & Cheney, R. E. Myosin-X knockout is semi-lethal and demonstrates that myosin-X functions in neural tube closure, pigmentation, hyaloid vasculature regression, and filopodia formation. *Sci Rep* **7**, 17354 (2017).
13. Summerbell, E. R. *et al.* Epigenetically heterogeneous tumor cells direct collective invasion through filopodia-driven fibronectin micropatterning. *Sci. Adv.* **6**, eaaz6197 (2020).
14. Miihkinen, M. *et al.* Myosin-X and talin modulate integrin activity at filopodia tips. *Cell Reports* **36**, 109716 (2021).
15. Watanabe, T. M., Tokuo, H., Gonda, K., Higuchi, H. & Ikebe, M. Myosin-X Induces Filopodia by Multiple Elongation Mechanism. *Journal of Biological Chemistry* **285**, 19605–19614 (2010).
16. Berg, J. S. & Cheney, R. E. Myosin-X is an unconventional myosin that undergoes intrafilopodial motility. *Nat Cell Biol* **4**, 246–250 (2002).
17. Liu, K. C., Jacobs, D. T., Dunn, B. D., Fanning, A. S. & Cheney, R. E. Myosin-X functions in polarized epithelial cells. *MBoC* **23**, 1675–1687 (2012).
18. Kenchappa, R. S. *et al.* Myosin 10 Regulates Invasion, Mitosis, and Metabolic Signaling in Glioblastoma. *iScience* **23**, 101802 (2020).
19. Wu, J.-Q. & Pollard, T. D. Counting Cytokinesis Proteins Globally and Locally in Fission Yeast. *Science* **310**, 310–314 (2005).

20. Malla, M., Pollard, T. D. & Chen, Q. Counting actin in contractile rings reveals novel contributions of cofilin and type II myosins to fission yeast cytokinesis. *MBoC* **33**, ar51 (2022).

21. Loiodice, I. *et al.* Quantifying Tubulin Concentration and Microtubule Number Throughout the Fission Yeast Cell Cycle. *Biomolecules* **9**, 86 (2019).

22. Sayyad, W. A. & Pollard, T. D. The number of cytokinesis nodes in mitotic fission yeast scales with cell size. *eLife* **11**, e76249 (2022).

23. Zhang, G. *et al.* Protein Quantitation Using Mass Spectrometry. in *Computational Biology* (ed. Fenyö, D.) vol. 673 211–222 (Humana Press, 2010).

24. Hummert, J. *et al.* Photobleaching step analysis for robust determination of protein complex stoichiometries. *MBoC* **32**, ar35 (2021).

25. Peuhu, E. *et al.* MYO10-filopodia support basement membranes at pre-invasive tumor boundaries. *Developmental Cell* **57**, 2350-2364.e7 (2022).

26. Umeki, N. *et al.* Phospholipid-dependent regulation of the motor activity of myosin X. *Nat Struct Mol Biol* **18**, 783–788 (2011).

27. Krugmann, S. *et al.* Cdc42 induces filopodia by promoting the formation of an IRSp53:Mena complex. *Current Biology* **11**, 1645–1655 (2001).

28. Alieva, N. O. *et al.* Myosin IIA and formin dependent mechanosensitivity of filopodia adhesion. *Nat Commun* **10**, 3593 (2019).

29. Korobova, F. & Svitkina, T. Arp2/3 Complex Is Important for Filopodia Formation, Growth Cone Motility, and Neuritogenesis in Neuronal Cells. *MBoC* **19**, 1561–1574 (2008).

30. Lebrand, C. *et al.* Critical Role of Ena/VASP Proteins for Filopodia Formation in Neurons and in Function Downstream of Netrin-1. *Neuron* **42**, 37–49 (2004).

31. Baboolal, T. G., Mashanov, G. I., Nenasheva, T. A., Peckham, M. & Molloy, J. E. A Combination of Diffusion and Active Translocation Localizes Myosin 10 to the Filopodial Tip. *Journal of Biological Chemistry* **291**, 22373–22385 (2016).

32. Meyen, D. *et al.* Dynamic filopodia are required for chemokine-dependent intracellular polarization during guided cell migration in vivo. *eLife* **4**, e05279 (2015).

33. Efremov, A. K. *et al.* Application of piconewton forces to individual filopodia reveals mechanosensory role of L-type Ca2+ channels. *Biomaterials* **284**, 121477 (2022).

34. Santos, A., Shauchuk, Y., Cichoń, U., Vavra, K. C. & Rock, R. S. How Actin Tracks Affect Myosin Motors. in *Myosins* (ed. Coluccio, L. M.) vol. 1239 183–197 (Springer International Publishing, 2020).

35. Aramaki, S., Mayanagi, K., Jin, M., Aoyama, K. & Yasunaga, T. Filopodia formation by crosslinking of F-actin with fascin in two different binding manners: Bundling Mechanisms of F-Actin by Fascin in Filopodia. *Cytoskeleton* **73**, 365–374 (2016).

36. Nagy, S. & Rock, R. S. Structured Post-IQ Domain Governs Selectivity of Myosin X for Fascin-Actin Bundles. *Journal of Biological Chemistry* **285**, 26608–26617 (2010).

37. Zhuravlev, P. I., Lan, Y., Minakova, M. S. & Papoian, G. A. Theory of active transport in filopodia and stereocilia. *Proc. Natl. Acad. Sci. U.S.A.* **109**, 10849–10854 (2012).

38. Mogilner, A. & Rubinstein, B. The Physics of Filopodial Protrusion. *Biophysical Journal* **89**, 782–795 (2005).

39. Wu, J.-Q., Kuhn, J. R., Kovar, D. R. & Pollard, T. D. Spatial and Temporal Pathway for Assembly and Constriction of the Contractile Ring in Fission Yeast Cytokinesis. *Developmental Cell* **5**, 723–734 (2003).

40. Medalia, O. *et al.* Organization of Actin Networks in Intact Filopodia. *Current Biology* **17**, 79–84 (2007).

41. Sofroniew, Nicholas *et al.* napari: a multi-dimensional image viewer for Python. (2022) doi:10.5281/ZENODO.3555620.